Polymer Chemistry

Accepted Manuscript

This is an *Accepted Manuscript*, which has been through the Royal Society of Chemistry peer review process and has been accepted for publication.

Accepted Manuscripts are published online shortly after acceptance, before technical editing, formatting and proof reading. Using this free service, authors can make their results available to the community, in citable form, before we publish the edited article. We will replace this *Accepted Manuscript* with the edited and formatted *Advance Article* as soon as it is available.

You can find more information about *Accepted Manuscripts* in the Information for Authors.

Please note that technical editing may introduce minor changes to the text and/or graphics, which may alter content. The journal's standard Terms & Conditions and the Ethical guidelines still apply. In no event shall the Royal Society of Chemistry be held responsible for any errors or omissions in this *Accepted Manuscript* or any consequences arising from the use of any information it contains.

ROYAL SOCIETY OF CHEMISTRY

www.rsc.org/polymers

Synthesis and Self-Organization of Azobenzene Containing Hemiphasmidic Side-Chain Liquid-Crystalline Polymers with Different Spacer Lengths

Yan-Shuang Xu,[a] Dong Shi,[a] Jun Gu,[b] Zhen Lei,[a] He-Lou Xie,[c] Ti-Peng Zhao,[a] Shuang Yang,*[,a] and Er-Qiang Chen*[,a]

[a] *Beijing National Laboratory for Molecular Sciences, Department of Polymer Science and Engineering and Key Laboratory of Polymer Chemistry and Physics of Ministry of Education, College of Chemistry and Molecular Engineering, Center for Soft Matter Science and Engineering, Peking University, Beijing 100871, China*

[b] *State Key Laboratory of Rare Earth Materials Chemistry and Applications, College of Chemistry and Molecular Engineering, Peking University, Beijing 100871, China*

[c] *Key Laboratory of Special Functional Polymer Materials of Hunan Province, College of Chemistry, Xiangtan University, Xiangtan 411105, Hunan Province, China*

Email address: eqchen@pku.edu.cn; shuangyang@pku.edu.cn

† Electronic supplementary information (ESI) available: Molecular characterization data, calculation of relative electron density map and core dimension of the supramolecular column, and phase structure characterization data.

Abstract

A series of new hemiphasmidic side-chain liquid crystalline (LC) polymer (P-*n*, *n* is the number of methylene units of spacer, *n* = 2, 6, 10, 14) were synthesized. The azobenzene containing hemiphasmidic mesogens are linked to polymethacrylate main-chain through flexible spacers. The chemical structures of monomers and

polymers were confirmed by various characterization techniques. All of P-*n*s exhibit enantiotropic LC phase behavior, which is influenced greatly by varying the spacer length. Specifically, P-2 and P-6 exhibit a hexagonal columnar (Φ_H) phase. As longer spacers are introduced, P-10 and P-14 can form a centered rectangular columnar (Φ_R) phase at low temperatures, which will change into Φ_H phase upon heating. The lattice dimensions of the columnar (Φ) phases are pretty large, approaching to 9 nm when *n* increases to 14. This indicates that the column of P-*n*'s Φ phase is constructed by several chains laterally assembled together. For P-10 and P-14, the transition of Φ_H-Φ_R may be associated with the change of chain numbers of the supramolecular column. As the transition temperature is close to the glass transition temperature, the kinetics of Φ_H-to-Φ_R transition of P-10 becomes very slow.

Introduction

Liquid crystalline (LC) polymer is a long standing topic of polymer science and engineering, not only because of its application in the areas such as engineering plastics, optical and electro-optical devices, but also due to many fundamental issues of polymer chemistry and physics.[1-3] Rich phase behaviors have been encountered in side-chain LC polymers (SCLCPs), which depend on the chemical structures of main-chain, side-chain, and how these two are connected together.[1,2] When the calamitic mesogens on side-chains are linked to the main-chain through flexible spacers, smectic (Sm) phases can be readily realized in SCLCPs.[4,5] Parallel packing of calamitic mesogens largely dominates the LC properties. The resultant layered structure of Sm phases can consist of alternatively packed sub-layers of main- and side-chain, exhibiting the feature of microphase separation.[6-9] Bearing discotic mesogens on the side-chains, SCLCPs can form columnar (Φ) phases, wherein the supramolecular columns are constructed by stacking the discotic mesogens together.[10-14] On the other hand, Φ phases of SCLCPs can also take the whole chain rather than the mesogens on side-chains as the building block.[15-20] The typical examples are mesogen-jacketed LC polymers (MJLCPs)[16,21] and dendronized polymers.[17,22,23] For MJLCPs, rod-like mesogens are laterally attached to every repeating unit of the main-chain through a very short spacer or even a single carbon-carbon bond.[16,21] Owing to the strong "jacketing effect" imposed by side-chains, the main-chain becomes quite extended.[16,24,25] The cylindrical MJLCPs can be further utilized to synthesize the rod-coil block copolymers.[26-31] The side-chain

"jacketing effect" also exists in dendronized polymers. Particularly, when the tapered or wedge-shaped "Percec-type" dendrons are employed, the dendronized polymers demonstrate strong self-assembly ability towards Φ phases.[18,22,32] The supramolecular column can possess a "core-shell" structure, as a result of the nano-segregation within the column.[18,33,34]

As the chemical structures of main- and side-chain can be tailored freely, SCLCP is an attractive platform for the development of advanced materials. Aiming to different applications, one can synthesize novel SCLCPs by incorporating different functional groups with different shapes into the side-chain. Recently, we are interested in hemiphasmidic SCLCPs.[35-42] The hemiphasmidic mesogen is composed of a rod-like moiety linked with a half-disk group at one end, of which the molecular design roots in phasmid or polycataner mesogen.[43] Combining a rigid rod at center and two half disks at both ends, phasmid small molecules may self-assemble into Sm and Φ phases.[44-48] Hemiphasmidic SCLCPs were first synthesized by Ringsdorf[35] and Percec.[36,40] With polysiloxane main-chain, the polymers exhibit either Sm or Φ phase, depending on the length of alkyl tails at the half-disk part. As we reported previously, hemiphasmidic SCLCPs with main-chains of polystyrene and polyphenylacetylene also show the same tail length dependence of LC phase. It is worthy to emphasize that periodicity of the ordered structures of hemiphasmidic SCLCPs is remarkably large (i.e., > 5 nm), owing to that the dimension of hemiphasmidic mesogens is larger than that of the conventional rod-like or discotic mesogens.[41,42] This feature makes hemiphasmidic SCLCPs the suitable candidate for the nanofabrication process of

nano-patterning. Interestingly, for the Φ phase of hemiphasmidic SCLCPs, we have noticed that the supramolecular column with the diameter larger than 5 nm shall be constructed by several chains laterally associated together.[41,42] Namely, the "multi-chain column" with the main-chains threading through the column center is the building block of Φ phase. This molecular packing scheme is very different from that of MJLCPs and many dendronized polymers, which take the "single-chain columns" to form the Φ phases.

In our former work, the hemiphasmidic mesogens are linked to the main-chain using short methylene ether bridges.[41,42] Here, we synthesize a new series of hemiphasmidic SCLCPs with the rod-like mesogen of azobenzene which may impart the polymer photoresponsive properties, such as photoinduced deformation[49] and optical anisotropy.[50] The azobenzene containing hemiphasmidic groups are linked to the polymethacrylate main-chains via flexible spacers with different lengths in these polymers (see Scheme 1, referred to as P-*n*, *n* is the number of methylene units on the spacer, *n* = 2, 6, 10, 14). In this paper, we focus on the phase structures and transitions of P-*n*. The flexible spacers can promote the dynamic decoupling between the main-chain and side-chain mesogens.[4,5,51] Additionally, adding spacer with different length to the wedge-like hemiphasmidic group may make the whole side-chain shape more variable. Therefore, in addition to the decrease of glass transition temperature (T_g) of P-*n* with increasing *n*, the LC properties of P-*n* should also have the spacer length dependence. Mainly on the basis of one- and two-dimensional (1D and 2D) X-ray diffraction (XRD) results, we identify that above room temperature P-2 and P-6

possess a single first order transition from a hexagonal columnar (Φ_H) phase to isotropic state. For P-10 and P-14, the longer spacer causes the samples to form a centered rectangular columnar (Φ_R) phase at low temperatures, which will transform to a Φ_H phase before isotropization. The lattice parameters of the Φ phases of P-*n* are large, indicating the existence of "multi-chain columns". For P-14, the column diameter approaches to 9 nm. The Φ_R-Φ_H transition should be associated with the reorganization of the supramolecular column.

Experimental section

Materials

2-Bromoethanol (J&K Chemical, 95%), 6-Bromo-hexanol (Energy Chemical, 97%), 10-Bromo-1-decanol (J&K Chemical, 95%), methacrylic anhydride (J&K Chemical, 94%), and tert-butyldimethylchlorosilane (J&K Chemical, 99%) were used as received. Benzoyl peroxide (BPO, Guangdong Chemical Reagents Co., A.R.) was recrystallization with ethanol before used. Chlorobenzene (Beijing Chemical Reagents Co., A.R.) was purified by washing with concentrated sulfuric acid to remove residual thiophenes, followed by washing with deionized water, 3% sodium carbonate solution and with deionized water again, and then dried with anhydrous calcium chloride before it was finally distilled. Tetrahydrofuran (THF, Beijing Chemical Reagents Co., A.R.) was refluxed over sodium and then distilled. Trimethylamine (TEA, Beijing Chemical Reagents Co., A.R.) was refluxed over potassium hydroxide and then distilled. All the other chemicals were commercially

available and used without further purification.

Instruments and measurements

^{1}H and ^{13}C NMR spectra were recorded on a Bruker ARX400 spectrometer at room temperature (400 and 100 MHz for ^{1}H NMR and ^{13}C NMR, respectively) using deuterated chloroform ($CDCl_3$) as the solvent and tetramethylsilane (TMS) as the internal standard. Elemental analysis was performed with an Elementar Vireo EL instrument. Mass spectra were recorded on a Bruker Apex IV FTMS spectrometer. Gel permeation chromatography (GPC) was carried out on a Waters 515 GPC instrument using THF as an eluent at a flow rate of 1.0 mL/min at 35 ℃. The GPC calibration curve was obtained with linear polystyrene standards. Thermogravimetric analysis (TGA) was conducted on a Q600 instrument. Density of the samples was measured using a flotation technique.

To detect phase transition behaviors of the samples, differential scanning calorimetry (DSC) measurements were carried out on a TA Q100 instrument in a nitrogen atmosphere. The samples with a typical mass of 3–5 mg were encapsulated in hermetically sealed aluminum pans. Birefringence and LC textures of samples were examined under a polarized optical microscopy (POM, Leica DML) with a Mettler hot stage (FP-90). The POM samples with the thickness of ~10 μm were prepared by compressing the polymers at isotropic state between a glass slide and a cover glass, and then were cooled to room temperature at a rate of 0.1 ℃/min.

1D XRD experiments were performed with the high-flux small-angle X-ray

scatting instrument (SAXSess, Anton Paar) equipped with a Kratky block-collimation system. An imaging plate was used as the detector, which covers the *q*-range from 0.06 to 29 nm^{-1} ($q = 4\pi\sin\theta/\lambda$, where λ is the wavelength of 0.1542 nm and 2θ the scattering angle). A temperature control unit (Anton Paar TCS300) in conjunction with the SAXSess was utilized to study the structure evolution as a function of temperature. 2D XRD experiments of the oriented samples were recorded on a Bruker D8 Discover diffractometer with GADDS as 2D detector. The low-angle 2D XRD experiments were carried out on the Nanostar U small-angle X-ray scattering instrument (Bruker AKS) equipped with 3 pinholes collimation system.

Synthesis

The synthetic route of monomers and polymers is shown in Scheme 1. Compound **1**, **2**, and **R-Cl** (R is the half-disk end group of the side-chain, see Scheme 1) were prepared according to literatures.[41,52] The synthetic procedures of compound **3** to **7** and P-*n* (using P-2 as the example) are described below. All the molecular characterization data of the intermediates, monomers and polymers are provided in the ESI.†

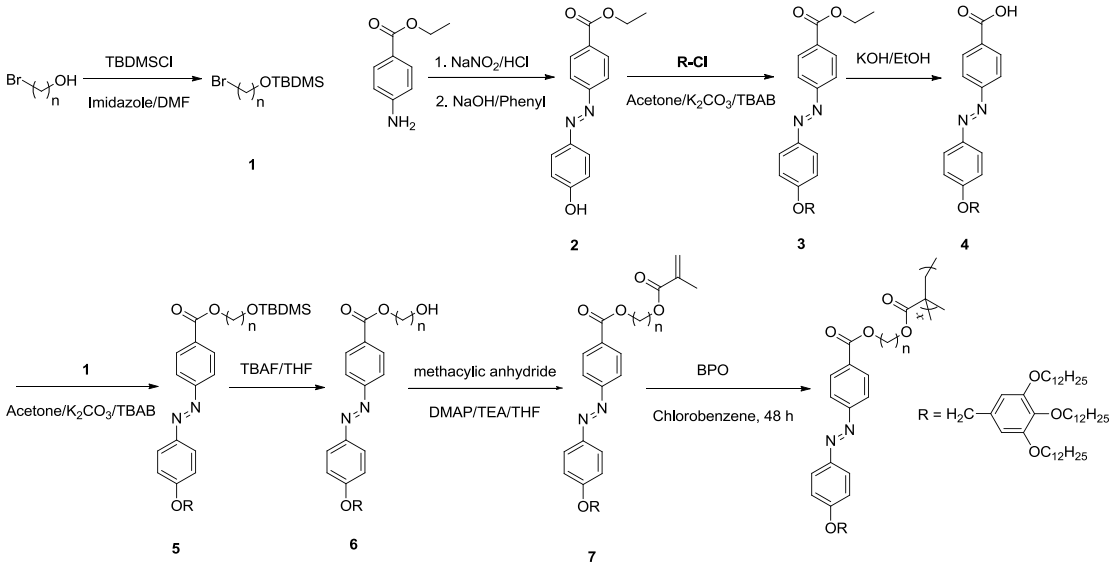

Scheme 1 Synthetic route of the monomers and polymers.

*Synthesis of **3***. To a 250 mL round-bottom flask was added **R-Cl** (3.6 g, 5.29 mmol), **2** (1.2 g, 4.44 mmol), K_2CO_3 (3.68 g, 26.7 mmol), catalytic amounts of KI, and 100 mL acetone. The mixture was refluxed overnight. The reaction mixture was cooled to room temperature, filtered to remove the insoluble salt which was washed with CH_2Cl_2. The filtrate was evaporated to dryness under a reduced pressure. The crude product was purified by column chromatography using petroleum ether/ethyl acetate (10/1, v/v) as eluent, affording **3** as yellow solid in 78.2% yield.

*Synthesis of **4***. 3 mL aqueous solution of KOH (1.23 g, 21.92 mmol) was added dropwise to a 100 mL ethanol solution of **3**, and the mixture was refluxed for 3 h. The reaction mixture was then evaporated to remove ethanol under a reduced pressure, and dissolved in THF. The mixture was adjusted the pH = 1 by addition of 1M HCl aqueous solution, extracted with diethyl ether, washed by distilled water to remove THF. The diethyl ether solution was dried over anhydrous $MgSO_4$, then evaporated to dryness under a reduced pressure to afford **4** as yellow solid in 85.6% yield.

*Synthesis of **5***. To a 250 mL round-bottom flask was added **4** (2.0 g, 2.26 mmol), **1** (*n* = 2, 0.62 g, 2.10 mmol), K_2CO_3 (3.0 g, 21.7 mmol), TBAB (300 mg) and 150 mL acetone. The mixture was refluxed overnight. After cooled to room temperature, the reaction mixture was filtered to remove the insoluble salt which was washed with CH_2Cl_2. The filtrate was evaporated to dryness under reduced pressure. The crude product was purified by column chromatography using petroleum ether/CH_2Cl_2 (1/2, v/v) as eluent, affording **5** as yellow solid in 78.2% yield.

*Synthesis of **6***. TBAF (0.551 g, 1.746 mmol) in 5 mL THF was added to a THF solution of **5** (*n* = 2, 0.96 g, 0.873 mmol), and the mixture was stirred at 25 ℃ for 2 h. The reaction mixture was then evaporated to dryness under a reduced pressure and dissolved in CH_2Cl_2. The mixture was washed with a saturated aqueous solution of NH_4Cl. An organic phase separated was dried over anhydrous $MgSO_4$ and evaporated to dryness under a reduced pressure. The crude product was purified by column chromatography using petroleum ether/ethyl acetate (5/1, v/v) as eluent, affording **6** as yellow solid in 91.9% yield.

*Synthesis of monomer **7***. To 50 mL THF solution of **6** (*n* = 2, 0.79 g, 0.080 mmol) and DMAP (48 mg, 0.40 mmol) was successively added methacrylic anhydride (1.76 mmol) and triethylamine (1.76 mmol), and the mixture was stirred at 50 ℃ for 6 h. Afterwards, the reaction mixture was concentrated under a reduced pressure, and diluted with CH_2Cl_2. The mixture was washed with a saturated aqueous solution of NH_4Cl, distilled water and brine. An organic phase separated was dried over anhydrous $MgSO_4$ and then evaporated to dryness under a reduced pressure. The

crude product was purified by column chromatography using petroleum ether/ethyl acetate (5/1, v/v) as eluent, affording **7** as yellow solid in 91.9% yield.

Polymerization of 7. Monomer **7** (*n* = 2, 300 mg, 0.258 mmol), BPO (0.312 mg, 0.0013 mmol) and 1 mL chlorobenzene were placed in a polymerization tube. After three freeze-pump-thaw cycles, the tube was sealed under vacuum and stirred at 90 ℃. After 24 h, the reaction mixture was poured into MeOH, and a yellow precipitate formed was collected by filtration. After removal the low molecular weight (MW) compounds, the obtained polymeric fraction was evaporated to dryness under a reduced pressure to give P-*n* (*n* = 2) as yellow solid in 50% yield.

Results

Synthesis and characterization

The synthetic route of the monomers (**7**) is shown in Scheme 1. In brief, compound **3** was firstly prepared via Williamson ether synthesis from ethyl 4-(4-hydroxyphenylazo) benzoate (**2**) and **R-Cl**, followed by hydrolyzation to the benzyl acid moiety (**4**). To introduce variable spacers between the main-chain and the side-chain, 1-bromoalkylanol protected by TBDMSCl (**1**) was used to react with **4**, followed by the deprotection of the trimethylsilyl to afford **6**. Finally, the monomer **7** was obtained through the reaction between **6** and methacrylic anhydride. The synthetic route towards **7** was proved to be effective, evidenced by the moderate to high yields of the intermediates and the final products of the monomers.

The polymers of P-*n*s were obtained through conventional free radical

polymerization of the azo-containing monomers initiated by BPO in chlorobenzene at 90 ℃. Yellow solids were obtained with good yield (37 % ~ 81 %, Table 1). All the obtained polymers could dissolve well in common solvent, such as THF, chloroform, toluene and dichloromethane. The MWs of P-*n*s were determined by GPC relative to polystyrene standards. Higher yields and higher MWs of P-10 and P-14 were obtained compared to those of P-2 and P-6, probably because the longer spacers relieved more the steric hindrance caused by the hemiphasmidic groups during polymerization.

Table 1 Yields and GPC results of P-*n* (*n* = 2, 6, 10, 14).

Polymer	Yield (%)	M_n (kDa)	M_w (kDa)	PDI
P-2	37	76	119	1.56
P-6	45	77	118	1.53
P-10	77	96	137	1.44
P-14	81	97	170	1.70

The chemical structures of P-*n* were confirmed by ^{1}H NMR spectroscopy. Fig. 1 compares the ^{1}H NMR result of P-14 with that of the monomer (M-14). The signals at 6.10 ppm, 5.55 ppm and 1.94 ppm are attributed to the propenyl and methyl protons in M-14, which disappeared after polymerization. The temperature for 5% weight loss of the polymers determined by TGA under nitrogen was found to be higher than 300 ℃, demonstrating their good thermal stability.

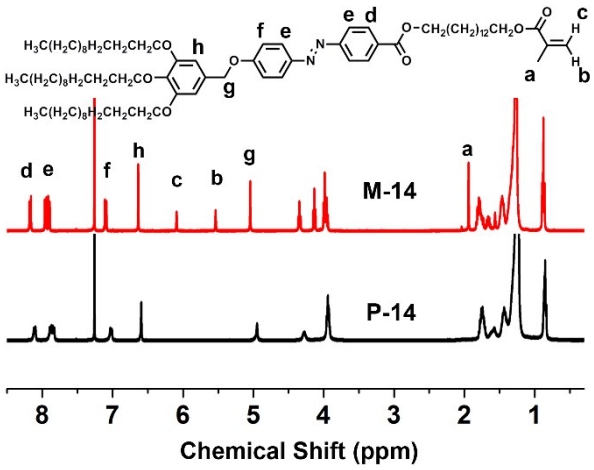

Fig. 1 ^{1}H NMR spectra of the monomer M-14 and the polymer P-14 in $CDCl_3$.

Phase structures of P-*n* at room temperature

Fig. 2a-d show the POM images of P-2, P-6, P-10 and P-14, respectively, obtained after the samples were cooled from isotropic melt to room temperature at a rate of 0.1 ℃/min. During cooling, the LC textures of P-2 and P-6 appeared rapidly when the temperature reached 120 and 100 ℃, respectively. For P-10 and P-14, the clear textures were observed after isothermal annealing the samples for relatively long time at room temperature, and were much smaller than that of P-2 and P-6 (Fig. 2). These observations demonstrated the LC properties of P-*n*, and also implied that the four samples bearing the spacers of different lengths might have distinct phase behaviors.

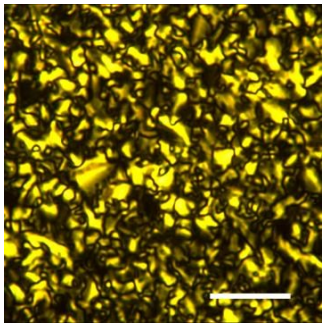
a

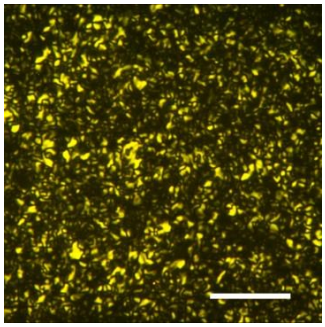
b

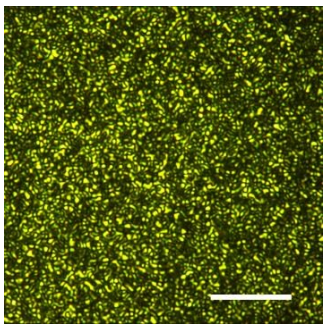
c

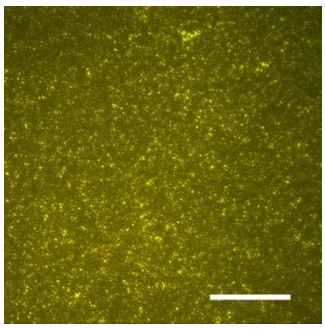
d

Fig. 2 POM images recorded at room temperature after the samples were slow cooled from isotropic melt. (a) P-2, (b) P-6, (c) P-10, (d) P-14. The scale bar: 1.0 μm.

We performed 1D XRD experiments to explore the LC structures of P-*n* at room temperature. Before measurement, the samples were also slowly cooled from isotropic state to room temperature. As shown in Fig. 3, P-*n*s render a typical amorphous halo in the high-angle region, reflecting the liquid-like short-range order on the sub-nanometer scale. On the other hand, the low-angle diffractions can be clearly observed. P-2 and P-6 exhibit the diffraction patterns quite different from those of P-10 and P-14. For P-2 and P-6, the diffraction peaks up to the fourth order with the *q*-ratio of 1:√3:2:√7 can be observed, manifesting the hexagonal packing. Combining the low- and high-angle diffraction results, we can conclude that P-2 and P-6 form Φ_H phase. P-10 and P-14 exhibit more low-angle diffraction peaks, of which the *q*-ratios are 1:1.20:1.84:2.24:2.40:3.42 and 1:1.20:2.10:2.38:3.31, respectively. The complex diffraction patterns preclude the possibility of smectic structures. Moreover, it also suggests that P-10 and P-14 form an Φ phase other than the simple Φ_H.

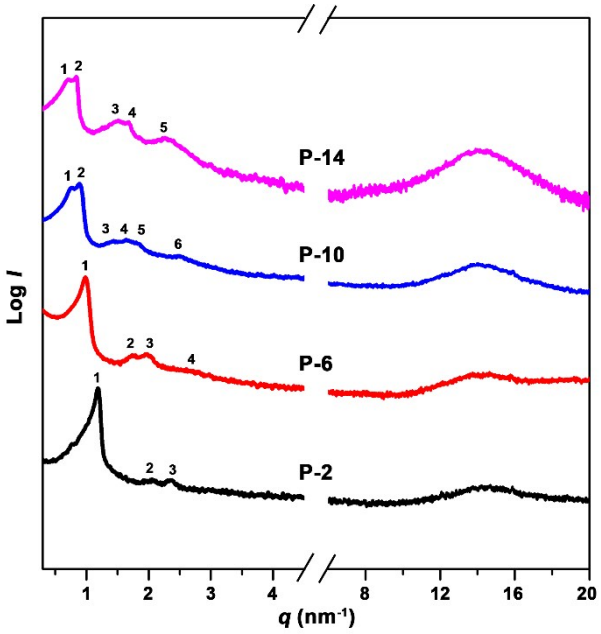

Fig. 3 1D XRD patterns of P-*n* (*n* = 2, 6, 10 and 14) recorded at room temperature.

To further unveil the LC phase structure of P-*n*, we carried out 2D XRD experiments of oriented samples. To obtain the aligned LC domains, the samples were mechanically sheared with mild external force at temperatures ~20 ℃ below the isotropic temperatures. Fig. 4a shows the schematic of the sheared sample, wherein the *z*- and *x*-axis represent the shearing direction and shearing gradient, respectively. Fig. 4b and 4c depict the 2D XRD patterns of sheared P-6. As shown in Fig. 4b, when the X-ray incident beam was perpendicular to the shear direction (*z*-axis), three low-angle diffraction peaks appear on *x*-axis, indicating the columns of Φ_H phase are aligned parallel to the shear direction. Fig. 4c presents the 2D XRD pattern recorded with the X-ray incident beam parallel to shear direction. The six arcs at q = 1.08 nm^{-1} demonstrate a 6-fold symmetry, confirming the hexagonal packing of the sample. This observation also indicates that the (10) plane of the hexagonal lattices is preferentially parallel to the substrate surface (i.e., *y*-*z* plane, see Fig. 4a). Combining the diffraction

patterns shown in both Fig. 4b and 4c, we consider that the sheared sample is still composed of polydomains rather than the monodomain, with an orientation distribution around the shearing direction. P-2 of the Φ_H phase presents the 2D XRD result similar to P-6 (see ESI†). The *a* parameters of hexagonal lattices are determined to be 6.07 and 7.25 nm for P-2 and P-6, respectively.

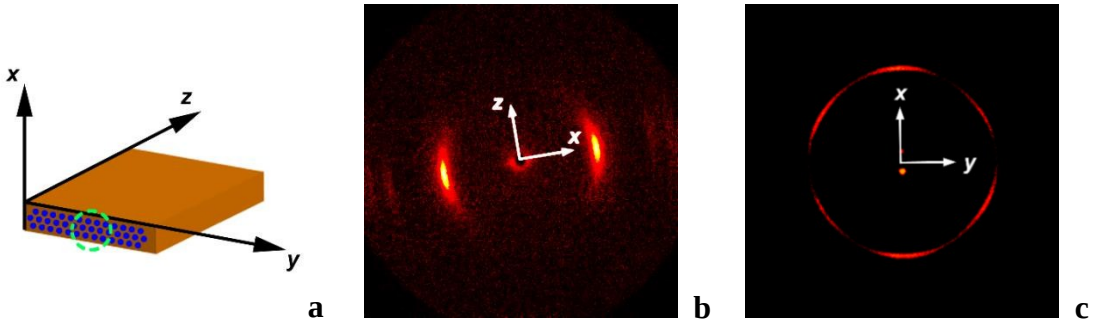

Fig. 4 (a) Schematic draw of the geometry of the sheared P-*n* samples. The *z*- and *x*-axis represent the shearing direction and shearing gradient, respectively. The dashed circle in (a) indicates the hexagonal packing of supramolecular columns. (b) and (c) 2D XRD patterns of oriented P-6. The X-ray beam was (b) perpendicular and (c) parallel to the shear direction (*z*-axis).

Fig. 5a-b show the 2D XRD results of the orientated P-10 sample. In Fig. 5a, the 2D XRD pattern was recorded with X-ray beam parallel to *y*-axis and thus perpendicular to the shear direction (*z*-axis). The pair of strong and relatively broad spots on the meridian (*x*-axis) is composed of two diffractions largely overlapping together, i.e., the peaks *1* and *2* shown on the 1D XRD profile (see Fig. 3). Careful examination can reveal that the other higher order diffractions with low intensity (i.e., peaks *3*, *4*, and *5*) are also appeared on the meridian. This observation confirms that mechanical shearing can result in uniaxial orientation of the sample. Fig. 5b depicts the 2D XRD pattern with the X-ray incident beam parallel to the shear direction (*z*-axis), wherein the *x*- and *y*-axis are along the equator and meridian, respectively.

According to the diffraction geometry, the very strong diffractions on the equator and in the quadrants can be assigned to (20) and (11) diffraction of a rectangular structure, corresponding to peak *1* and peak *2* in the 1D XRD pattern (see Fig. 3). The lattice parameters are thus calculated to be a = 17.3 nm and b = 7.86 nm. Consequently, all the other diffractions can be well indexed (see Fig. 5b). This outcome indicates that P-10 at room temperature adopts a centered rectangular columnar phase (Φ_R) of *c*2*mm* symmetry. After shearing, the column axis is parallel to the shear direction and moreover, the *a*-axis of Φ_R lattice is largely collinear with the shear gradient (*x*-axis). Fig. 5c shows the 2D XRD pattern of orientated P-14 with X-ray incident beam parallel to shear direction. It can be seen that P-14 also form a Φ_R phase, of which the lattice parameters are a = 14.98 nm and b = 11.18 nm.

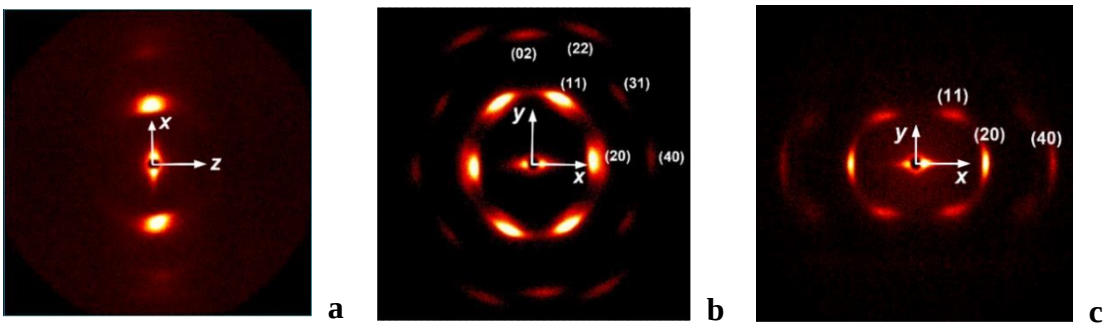

a **b** **c**

Fig. 5 2D XRD patterns of oriented P-10 (a, b) and P-14 (c). The X-ray incident beam was aligned perpendicular (a) and parallel (b, c) to the shear direction (*z*-axis).

Phase transition behaviors

Phase transition behaviors of P-*n*s were first studied by DSC. Fig. 6 depicts the second heating traces of P-*n*s at a rate of 10 ℃/min. Below room temperature there is a broad endothermic process with the transition temperature increased with increasing *n*. This shall be associated with the melting of ordered packing of alkyl tails formed

upon cooling P-*n* with different LC phases to sufficiently low tempeartures. For the transition form LC to isotropic state, it is observed that the endothermic peak shifts to lower temperature as *n* is increased, and the peak temperatures (T_is) of the four samples are of 138, 107, 73, and 70 ℃, respectively. The DSC results also indicate that P-*n* with longer spacer possesses lower T_g. For *n* = 2, 6, 10, the values of T_g are measured to be around 75, 45, and 35 ℃. For P-14, as the alkyl tail melting largely overlaps with the glass transition, its T_g cannot be clearly detected by DSC. Combining the dynamic mechanical analysis (DMA) result (see ESI†), we suggest that the T_g of P-14 should be around 20 ℃.

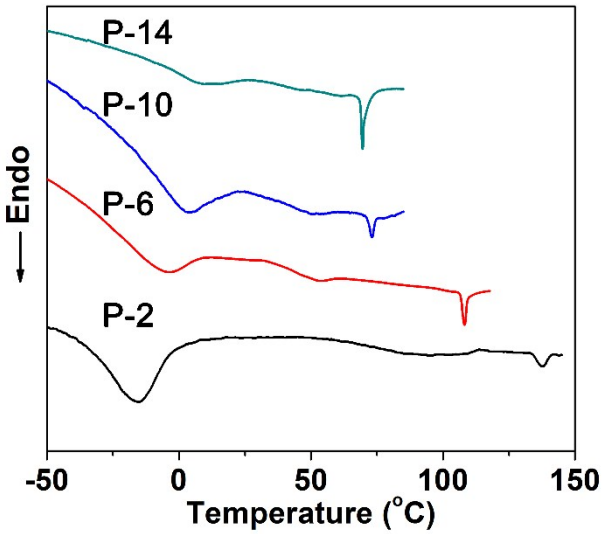

Fig. 6 DSC traces of P-*n* (*n* = 2, 6, 10 and 14) upon the second heating at a rate of 10 ℃/min.

We further investigated the LC phase transition of P-*n* using temperature dependent XRD experiments. The structural evolution of P-2 and P-6 looks relatively simple. Namely, at low temperatures, the samples formed the Φ_H phase as discussed above; when the temperature was higher than their T_i, the first diffraction peaks became a halo and the high order diffraction peaks disappeared, suggesting that P-2

and P-6 became isotropic (see ESI†). Upon cooling, the samples returned to Φ_H, demonstrating the enantiotropic LC behavior.

P-10 and P-14 exhibited more complex phase transitions. The 1D XRD patterns of P-10 recorded at various temperatures upon heating are shown in Fig. 6a. When the temperature exceeds 55 ℃, the diffraction profile in the low-angle region becomes substantially different from that at lower temperatures, which shows the *q*-ratio of 1:√3:2:√7, featuring the Φ_H phase. Therefore, we conclude that P-10 possesses a transition from Φ_R to Φ_H upon heating. This transition is not detected by DSC experiment, which may be due to that the latent heat of the Φ_R-to-Φ_H transition is very small. As the temperature is increased to above 80 ℃, a scattering halo instead of narrow diffraction peak is observed in the low-angle region, indicating the isotropic state. Upon heating, P-14 renders the phase transition similar to P-10. As shown in Fig. 7b, the transitions of Φ_R-to-Φ_H and Φ_H-to-isotropic occur at around 60 ℃ and 70 ℃, respectively.

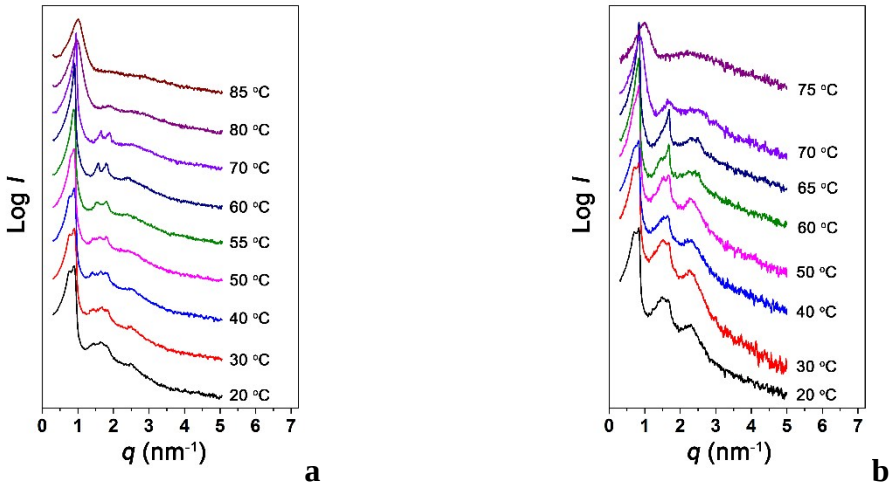

Fig. 7 Sets of 1D XRD profiles of (a) P-10 and (b) P-14 recorded at various temperatures upon heating.

Upon cooling, the transition from Φ_H to Φ_R of both P-10 and P-14 can be

evidenced by XRD experiment, however, the transition kinetics of these two are quite different. Fig. 8a shows the change of 1D XRD patterns of P-10 during cooling. The Φ_H phase forms quickly when the temperature reached the T_i (i.e., ~73 ℃). When the temperature became lower than the 55 ℃, the Φ_R phase cannot be directly obtained, although at those temperatures the Φ_R phase is the most stable LC phase. Continuous cooling just leads to peak broadening. The characteristic diffractions of Φ_R are not clear at room temperature, implying that the Φ_H-to-Φ_R transition of P-10 is incomplete. This outcome suggests that the formation of Φ_R of P-10 is kinetically slow. However, we found that isothermal annealing at properly selected temperatures could promote the formation of Φ_R phase of P-10. For example, keeping the sample at 45 ℃, we observe that the first diffraction gradually separates into two when the annealing time is prolonged (Fig. 8b). For P-14, the Φ_H-to-Φ_R transition kinetics is rapid. The Φ_H and Φ_R phase of P-14 can form once the temperature decreased to the corresponding phase transition temperature upon cooling (Fig. 8c).

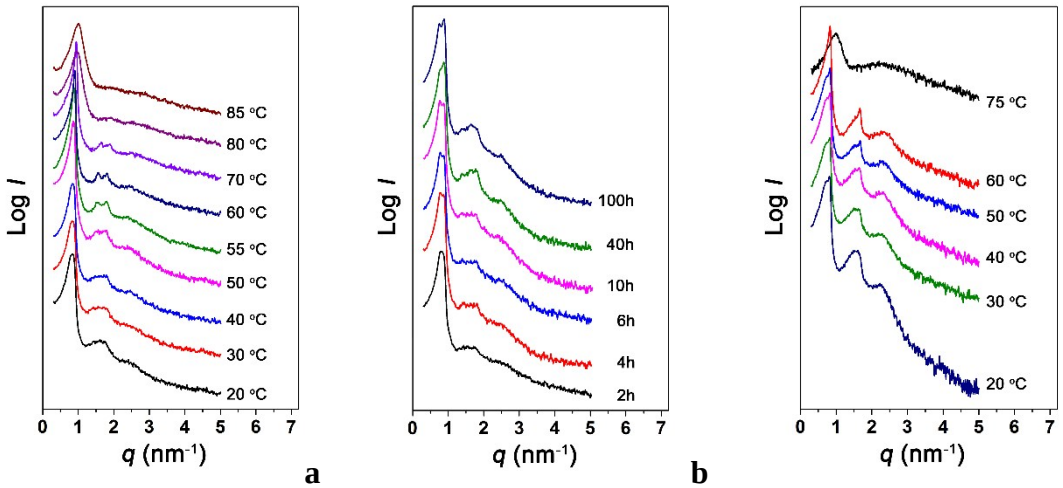

Fig. 8 The XRD patterns recorded for P-10 (a) and P-14 (c) upon cooling, and P-10 (b) during isothermal annealing at 45 ℃.

Discussion

Molecular packing scheme

Aforementioned, P-*n*s containing spacers with different lengths exhibit different phase behaviors. At room temperature, P-2 and P-6 possess Φ_H phase, while P-10 and P-14 form Φ_R phase. For P-10 and P-14, besides the isotropization at around 70 ℃, an additional transition of Φ_R-to-Φ_H occurs at above 50 ℃ during heating. This phase transition is reversible, but during cooling it requires quite long time for P-10. Table 2 summarizes the phase structures, transition temperatures (T_{trans}) and the lattice parameters of P-*n*s. One important question is how the chains of P-*n* pack together, which strongly depends on the spacer length of *n*, in the LC phases.

Table 2 Transition temperatures and structure analysis of P-*n* (*n* = 2, 6, 10 and 14)

	T_g[a] (℃)	T_{trans} (℃)	Phase	Lattice parameters[b] (nm)	ρ[c] (g cm^{-3})	μ[d]	Z[e]
P-2	75	138[a]	Φ_H	a = 6.07	1.02	8.6	~4
P-6	45	107[a]	Φ_H	a = 7.25	1.02	11.7	~6
P-10	35	~55[b]	Φ_R	a = 17.30, b = 7.86	1.02	16.5	~8
		73[a]	Φ_H	a = 8.03	~1.02	13.6	~7
P-14	~20	~60[b]	Φ_R	a = 14.98, b = 11.18	1.01	19.2	~10
		70[a]	Φ_H	a = 8.65	~1.01	14.9	~8

[a] Determined by DSC. For P-14, DMA method was also used. [b] Estimated from XRD results. [c] Experimental density measured at 25 ℃. [d] Number of repeat monomer per column stratum, $\mu = N_A S\rho t/M_{rep}$, where N_A is Avogadro's number, S is the cross section area of each column, M_{rep} is the molecular weight of repeating unit, t is the average height of column stratum which is assumed to be 0.44 nm. [e] Number of chains involved in one column, $Z \approx \mu/2$.

As shown by the chemical structure of P-*n*, the wedge-shaped hemiphasmidic group is attached to the polymethacrylate backbone via a flexible spacer. Accordingly, similar to the cases of other side-chain polymers in Φ phases, it can be considered that once the P-*n* chains self-assemble into an Φ phase the main-chain will thread through

the column center surrounded by the side-chains.[22,53] The side-chain orientation relative to the main-chain can be inferred from 2D XRD experiment. Fig. 9a and 9b are the 2D XRD patterns covering the high-angle region of sheared P-6 and P-10 at 20 ℃. While the (*hk*) diffractions of Φ phase close to beam stop appear on the *x*-axis, the scattering halo maximized at 0.44 nm, which is mostly contributed by the interference of the side-chains, is more or less concentrated on the shear direction (*z*-axis). Therefore, the side-chains are preferentially perpendicular to the column axis and thus the main-chain. The 2D XRD pattern of Fig. 9c was recorded after the sheared P-10 was heated to 60 ℃. Compared to Fig. 9b of P-10 in Φ_R, the (*hk*) diffractions and the high-angle scattering of P-10 in Φ_H remain on *x*- and *z*-axis, respectively. This suggests that the orientations of main- and side-chain are almost unchanged during the transition from Φ_R to Φ_H.

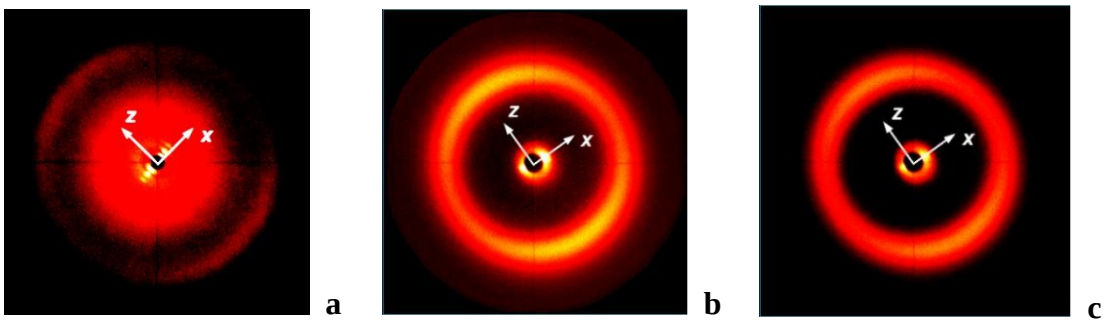

a **b** **c**

Fig. 9 2D XRD patterns of (a) P-6, (b) P-10 at 20 ℃ and (c) P-10 at 60 ℃ recorded with X-ray perpendicular to the shear direction (*z*-axis). The scatterings concentrated on *z*-axis in high-angle region correspond to the *d*-spacing of ~0.44 nm.

The XRD results suggest that the P-*n* column should have electron density variation along the radius direction, which is associated with the nano-segregation of different components within the column. We calculated the relative electron density maps based on the 1D XRD data. Fig. 10a gives the result of P-10 in its Φ_H phase.

According to the chemical structure of P-10, we presume that the blue colored area with the low electron density should correspond to alkyl tails on the periphery of the columns. The green colored ring with intermediate electron density is assigned to the azobenzene moieties, of which the width is of ~1 nm, in agreement with the length of the rod-like mesogen. In this case, the circle area at the column center with red and yellow color should be occupied by the main-chain, aliphatic spacers, and the ester group linked with azobenzene. This area possesses the highest electron density within the column, which may be due to that the small area (diameter of ~ 4 nm) includes two –OCO– groups on each repeating unit. It is interesting to note that area occupied by the rod-like azobenzene groups in the Φ_H phase bears a relatively lower electron density. This can be caused by that the rod-like mesogens along the radial direction are sprayed from each other, and thus are not parallel packed together. Fig. 10a of P-10 indicates a "core-shell-corona" structure for the column, which can be found in the other three P-*n*s.

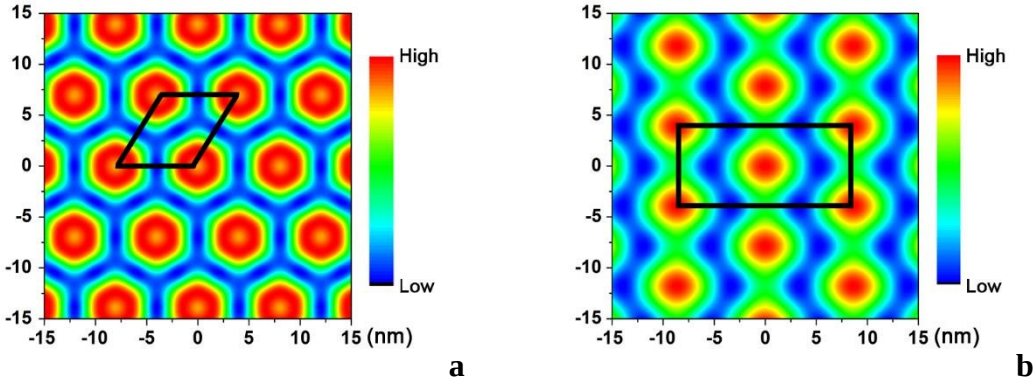

Fig. 10 The relative electron density map of P-10 with (a) hexagonal columnar phase and (b) rectangular columnar phase calculated based on XRD results.

Fig. 10b presents the relative electron density map of the rectangular lattice of P-10. In the Φ_R phase with *c*2*mm* symmetry, the lattice contains two columns. The

cross section of column's core (red colored) becomes more like an ellipsoid, which elongates along the *a*-axis and slightly shrinks along the *b*-axis. The polymethacrylate main-chain shall again occupy the column center, giving the highest electron density. The green area with relatively low electron density is also ellipsoid-like, where the unparallel azobenzene groups reside in. As the Φ_R phase exists in P-10 and P-14 but not in P-2 and P-6, the long alkyl spacers should play a critical role, which will be discussed later.

It is noteworthy that P-*n*s possess pretty large lattice dimensions of their Φ phases (see Table 2). For example, the *a* parameter of P-14's Φ_H phase approaches to 9 nm. Regarding to such a large lattice, of particular interest is how many repeating units are required to fill the space. Taking one column stratum with a thickness of *t*, the number of repeating units (μ) packed therein can be calculated as: $\mu = N_A St\rho/M_{rep}$, where N_A is Avogadro's number, *S* is the cross section area of each column, ρ is the density, and M_{rep} is the molar mass of repeating unit. On the basis of the 2D XRD pattern shown in Fig. 9, we assume *t* of 0.44 nm, which represents fairly the thickness of side-chain. The values of ρ were measured at room temperature by the floating method. To estimate the ρ of P-10 and P-14 with Φ_H phase, the samples were quenched rapidly from 60 to 20 ℃. The calculation result of μ is listed in Table 2, which is remarkably larger in comparison with MJLCPs and some other dendronized polymers.[22,23] Moreover, as the spacer becomes longer, μ increases significantly. For the Φ_H phase, the values of μ are of 8.6 for P-2 and of 14.9 for P-14. For the Φ_R phase, P-10 and P-14 possess even larger μ of 16.5 and 19.2, respectively. In our previous

work,[41,42] we propose that the large μ in fact suggests that the column in Φ phases of side-chain polymers is constructed by several chains instead of single chain. If assuming that the Φ phase of P-*n* takes the "single chain column" as its building block, increase of μ with increasing *n* should reflect that more repeating units connected in sequence on a same chain will be squeezed into the column unit. In this case, a pretty long segment of main-chain, e.g., ~15 repeating units of P-14, would be compressed into a 0.44 nm thick space. This is physically unreasonable. One should be aware of that the longer spacer of P-*n* in fact makes the side-chain larger, which can impart stronger steric hindrance around the main-chain. This will lead to more extended conformation of P-*n* so that the chain becomes harder to be compressed. In this case, we consider that the building block of the Φ phases shall be "multi-chain column" of P-*n* composed of several chains laterally associated together. Furthermore, considering that the dimension of ~0.44 nm is roughly the projection length of backbone with two repeating units on the column axis,[24] the number of chains involved in each column (*Z*) is nearly a half of μ (see Table 2).

On the basis of data listed in Table 2, we can further estimate the volume occupied by each repeating unit (V_{rep}) in the Φ phase: $V_{rep} = St/\mu$. Fig. 11a shows the plot of V_{rep} vs. *n*, wherein a linear relationship is obtained. The slope indicates that the volume of each methylene units is of ~0.023 nm^3, fairly agreeing with that evaluated for polyethylene in melt state.[54] As the side-chain of P-*n* is orthogonal to the column axis, the column radius of Φ_H (R_H), which is a half the *a* dimension, shall be mainly determined by the side-chain length. Fig. 11b describes R_H as a function of *n*. In

addition, based on the volume fraction, we estimated the radius of the core domain (R_C) occupied by the polymethacrylate main-chain and spacer within the column of Φ_H (see ESI†), of which the results are also shown in Fig. 11b. The difference of ~2 nm between R_H and R_C, which can represent the length of hemiphasmidic group, remain nearly a constant for the four samples studied. On the other hand, the increase of R_H and R_C with increasing n gradually becomes slower for larger n. This shall be mainly because the longer spacer adopts more *gauche* conformation.

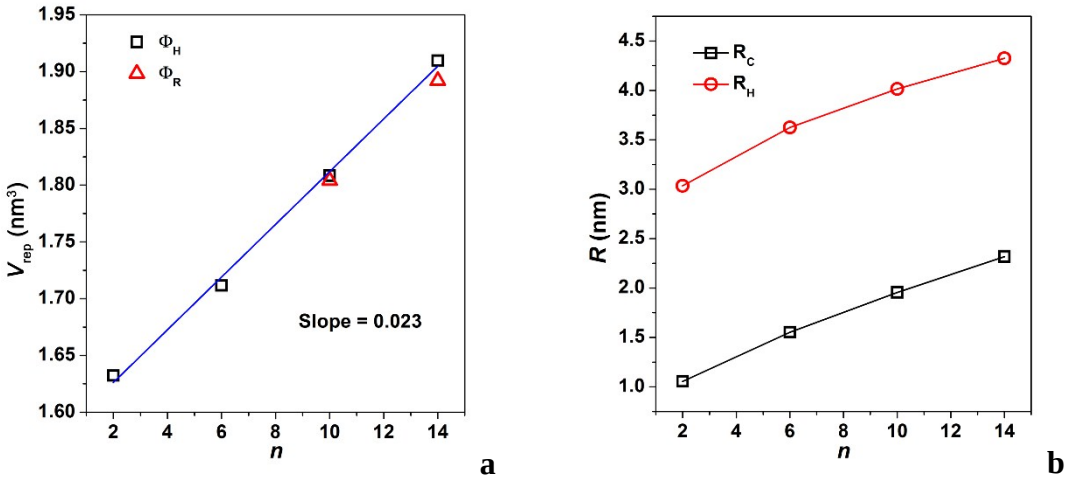

Fig. 11 (a) Volume of repeating unit V_{rep} and (b) column radius R_H and core radius R_C as functions of the spacer length n. In (a), the V_{rep} data of both Φ_H (black square) and Φ_R (red triangle) are plotted for P-10 and P-14.

The Φ_R-Φ_H transition.

For P-*n* studied, it is of particular interest that P-10 and P-14 can exhibit Φ_R and Φ_H phase, while the samples with shorter spacer only can form Φ_H phase. The comparison indicates that the Φ_R formation shall be related to the length of spacer. The hemiphasmidic group itself is wedge-shaped. After a long methylene sequence is linked at one end of rod-like moiety, the resultant side-chain of P-*n* will have the shape affected by the conformation of spacer. We presume that the Φ_R formation and

Φ_R-Φ_H transition is largely related to the conformation change of flexible spacer. To seek the close packing and thus to minimize the free energy, the long spacers with increased internal freedom of rotation may extend in one direction at low temperatures. This will result in the columns more ellipsoid-like, in favor of the packing of Φ_R phase.

To examine the conformation variation of flexible spacers, we performed FT-IR experiment. Fig. 12a shows the FT-IR spectra of P-10 at various temperatures upon heating. The two bands at 1467 and 1460 cm^{-1} can be assigned to the methylene sequence with a *trans*-dominant and a *gauche*-dominant conformation, respectively.[55] During heating, intensity of the band at 1460 cm^{-1} gradually increases while that at 1467 cm^{-1} decreases. This observation indicates that the methylene units adopt more *gauche* conformation at higher temperatures. Using the IR intensities obtained by spectral deconvolution, the ratio of peak area at 1467 cm^{-1} to that at 1460 cm^{-1} (A_{1467}/A_{1460}) can be obtained, which decreased from 1.44 to 1.07 when the temperatures increased from 26 to 70 ℃. Fig. 12 presents the plot of $\ln(A_{1467}/A_{1460})$ vs. the reciprocal of temperature ($1/T$), wherein two linear lines can be seen. It is noted that the slope changes at ~55 ℃, in consistent with the transition temperature of Φ_H-to-Φ_R detected by 1D XRD in the heating experiment. In this case, although the IR absorptions at 1467 cm^{-1} and 1460 cm^{-1} include the contribution from both the spacer and alkyl tails, we can still infer that the conformation of the spacer becoming more *gauche* is a main reason for the Φ_R-to-Φ_H transition.

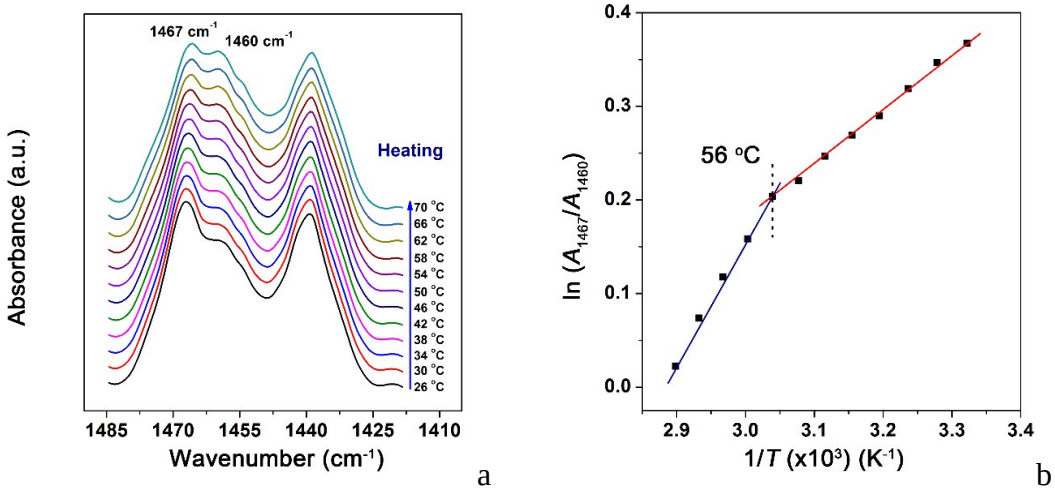

Fig. 12 (a) FT-IR spectra of P-10 recorded at various temperatures during heating. (b) Plot of ln(A_{1467}/A_{1460}) vs. 1/T. A_{1467} and A_{1460} are the peak area of the two bands at 1467 and 1460 cm^{-1}.

Recently, it is reported that the polymers dendronized with semifluorinated janus dendrimers may undergo a Φ_R-Φ_H transition upon heating, accompanying with an enlargement of the column cross section and a slight increase of the number of repeating units packed in a column unit.[32] For P-*n*, the Φ_R-Φ_H transition results in a significant reduction of the column cross section area *S*. The *S*-ratios of Φ_R to Φ_H are of ~1.2 and ~1.3 for P-10 and P-14, respectively (see Table 2). While the side-chains remain the orientation perpendicular to column axis as evidenced by Fig. 9b and 9c, the shrinkage of column area caused by the transition from Φ_R to Φ_H might be resulted from the contraction of side-chain and simultaneously the extension of backbone. In this case, the chain number of each column could remain unchanged. However, more likely, there is a possibility that the number of chains in the column changes. At above T_g, the polymer chains in LC phases are still mobile, and thus the reorganization of "multi-chain column" may occur. As mentioned above, with the Φ_H phase as the precursor, the Φ_R phase formation of P-10 upon cooling is rather slow.

This slow process may be related to the migration of chains during the phase transition. Once the chains leave a destroyed column to join a survived one nearby, the new column with increased number of chains appears in the Φ_R phase. We found that the Φ_R phase formation of P-10 was largely dependent on temperature. After rapidly cooled to below 30 ℃, even isothermal annealing for more than several days would hardly lead to the Φ_R phase. This should be due to that at below the T_g of 35 ℃ the chain mobility was greatly reduced. P-14 possesses the T_g lower and the Φ_R-Φ_H transition temperature higher than P-10. It can form the Φ_R much easier than P-10. This comparison supports that the chain mobility is critical for the Φ_H-Φ_R transition.

Conclusion

In summary, we synthesized a new series of hemiphasmidic SCLCPs (P-*n*s), of which the hemiphasmidic mesogen bearing azobenzene group is linked to the polymethacrylate main-chain via flexible spacers. Increasing the methylene unit number *n* of the spacers leads to the significant decrease of T_g. More importantly, we demonstrate that the LC properties of P-*n* depend greatly on the spacer length. As evidenced by XRD results, P-2 and P-6 just exhibit the Φ_H phase of *p*6*mm* symmetry. With longer spacers, P-10 and P-14 can form the Φ_R phase with *c*2*mm* symmetry at low temperatures, which will transform into Φ_H phase before isotropization. All the Φ phases present pretty large lattice dimensions, which approaches to 9 nm when *n* increases to 14. In this case, the supramolecular column of P-*n* shall contain several chains laterally associated together. Namely, for the Φ phases of P-*n* observed,

"multi-chain columns" rather than "single-chain columns" act as the building block. The supramolecular column in Φ_R phase is more ellipsoidal, which may be caused by that the long spacer with more *trans* conformation at lower temperatures makes the side-chain more elongated. Thermal FT-IR experiment infers that the Φ_R-to-Φ_H transition upon heating is associated with conformation transformation of the spacer changes from *trans*-dominated to *gauche*-dominated. For the column units with a same thickness, we note that the Φ_R phase possesses the number of repeating unites greater than the Φ_H phase. This outcome suggests that during the Φ_R-Φ_H transition there is a reorganization process of the supramolecular column, resulting in the numbers of the chains involved in the column changed. The kinetics of the reorganization process is dependent of the mobility of chains. The Φ_R phase formation of P-10 upon cooling is pretty slow, which may be due to the slowing down chain dynamics at the temperatures near the glass transition. We anticipate that the Φ phases of P-*n*s can be employed in construction of ordered thin films with the periodicity of 5 – 10 nm. As the azobenzene moiety can undergo reversible *trans*-*cis* isomerization under photoirradiation, the P-*n* films should be able to render photo-responsive properties. The corresponding research is currently carried out in our laboratory.

Acknowledgments

This work was supported by the National Natural Science Foundation of China (NNSFC Grants 51273002, 21474002, 20990232, and 21474005). We thank Dr. M.-Q. Ren and Dr. C. Zheng at SINOPEC Beijing Research Institute of Chemical Industry

for their help in the 2D XRD experiments.

Notes and references

1 D. J. Simmonds, *Liquid Crystal Polymers, From Structures to Applications*, Elsevier Applied Science, 1992.

2 X.-J. Wang and Q.-F. Zhou, *Liquid Crystalline Polymers*, World Scientific Publishing Co. Pte. Ltd, 2004.

3 C.-S. Hsu, *Prog. Polym. Sci.*, 1997, **22**, 829-871.

4 H. Finkelmann, H. Ringsdorf and J. H. Wendorff, *Makromol. Chem.*, 1978, **179**, 273-276.

5 H. Finkelmann, H. Ringsdorf, W. Siol and J. H. Wendorff, *Makromol. Chem.*, 1978, **179**, 829-832.

6 P. Davidson, *Prog. Polym. Sci.*, 1996, **21**, 893-950.

7 X.-Q. Zhu, J.-H.Liu, Y.-X.Liu and E.-Q. Chen, *Polymer*, 2008, **49**, 3103-3110.

8 Z.-Q. Yu, T.-T. Li, Z. Zhang, J.-H. Liu, W. Z. Yuan, J. W. Y. Lam, S. Yang, E.-Q. Chen and B. Z. Tang, *Macromolecules*, 2015, **48**, 2886-2893.

9 J. P. Cotton and F. Hardouin, *Prog. Polym. Sci.*, 1997, **22**, 795-828.

10 W. Kreuder and H. Ringsdorf, *Makromol. Chem. Rapid Commun.*, 1983, **4**, 807-815.

11 C. Xing, J. W. Y. Lam, K. Zhao and B. Z. Tang, *J. Polym. Sci., Part A: Polym. Chem.*, 2008, **46**, 2960-2974.

12 A. F. Thünemann, S. Kubowicz, C. Burger, M. D. Watson, N. Tchebotareva and K. Müllen, *J. Am. Chem. Soc.*, 2003, **125**, 352-356.

13 P. H. J. Kouwer, W. F. Jager, W. J. Mijs and S. J. Picken, *Macromolecules*, 2000, **33**, 4336-4342.

14 B. Mu, B. Wu, S. Pan, J. Fang and D. Chen, *Macromolecules*, 2015, **48**, 2388-2398.

15 G. Ungar, *Polymer*, 1993, **34**, 2050-2059.

16 X.-F. Chen, Z. Shen, X.-H. Wan, X.-H. Fan, E.-Q. Chen, Y. Ma and Q.-F. Zhou,

Chem. Soc. Rev., 2010, **39**, 3072-3101.

17 J. G. Rudick and V. Percec, *Acc. Chem. Res.*, 2008, **41**, 1641-1652.

18 B. M. Rosen, C. J. Wilson, D. A. Wilson, M. Peterca, M. R. Imam and V. Percec, *Chem. Rev.*, 2009, **109**, 6275-6540.

19 H.-J. Sun, S. Zhang and V. Percec, *Chem. Soc. Rev.*, 2015, **44**, 3900-3923.

20 K.-P. Liu, Z.-Q. Yu, J.-H. Liu and E.-Q. Chen, *Macromol. Chem. Phys.*, 2009, **210**, 707-716.

21 Q. F. Zhou, H. M. Li and X. D. Feng, *Macromolecules*, 1987, **20**, 233-234.

22 Y. K. Kwon, S. Chvalun, A.-I. Schneider, J. Blackwell, V. Percec and J. A. Heck, *Macromolecules*, 1994, **27**, 6129-6132.

23 V. Percec, J. Heck, D. Tomazos, F. Falkenberg, H. Blackwell and G. Ungar, *J. Chem. Soc., Perkin Trans. 1*, 1993, 2799-2811.

24 C. Ye, H.-L. Zhang, Y. Huang, E.-Q. Chen, Y. Lu, D. Shen, X.-H. Wan, Z. Shen, S. Z. D. Cheng and Zhou, Q.-F. *Macromolecules*, 2004, **37**, 7188-7196.

25 X.-Y. Yin, C. Ye, X. Ma, E.-Q. Chen, X.-Y. Qi, X.-F. Duan, X.-H. Wan, S. Z. D. Cheng and Q.-F. Zhou, *J. Am. Chem. Soc.*, 2003, **125**, 6854-6855.

26 P. Gopalan, Y. Zhang, X. Li, U. Wiesner and C. K. Ober, *Macromolecules*, 2003, **36**, 3357-3364.

27 Yi, X. Fan, X. Wan, L. Li, N. Zhao, X. Chen, J. Xu and Q.-F. Zhou, *Macromolecules*, 2004, **37**, 7610-7618.

28 C. Y. Li, K. K. Tenneti, D. Zhang, H. Zhang, X. Wan, E.-Q. Chen, Q.-F. Zhou, A.-O. Carlos, S. Igos and B. S. Hsiao, *Macromolecules*, 2004, **37**, 2854-2860.

29 K. K. Tenneti, X. Chen, C. Y. Li, Y. Tu, X. Wan, Q.-F. Zhou, I. Sics and B. S. Hsiao, *J. Am. Chem. Soc.*, 2005, **127**, 15481-15490.

30 X.-B. Liu, Y.-F. Zhao, X.-H. Fan and E.-Q. Chen, *Chin. J. Polym. Sci.*, 2013, **31**, 946-958.

31 F. Zhou, Q.-H. Zhou, H.-J. Tian, C.-S. Li, Y.-D. Zhang, X.-H. Fan and Z.-H. Shen, *Chin. J. Polym. Sci.*, 2015, **33**, 709-720.

32 V. Percec, M. R. Imam, M. Peterca and P. Leowanawat, *J. Am. Chem. Soc.*, 2012, **134**, 4408-4420.

33 G. Ungar, D. Abramic, V. Percec and J. A. Heck, *Liq. Cryst.*, 1996, **21**, 73-86.

34 X. Chen, K. K. Tenneti, C. Y. Li, Y. Bai, R. Zhou, X. Wan, X. Fan and Q.-F. Zhou, *Macromolecules*, 2006, **39**, 517-527.

35 C. Lin, H. Ringsdorf, M. Ebert, R. Kleppinger and J. H. Wendorff, *Liq. Cryst.*, 1989, **5**, 1841-1847.

36 V. Percec and J. Heck, *Polym. Bull.*, 1990, **24**, 255-262.

37 V. Percec and J. Heck, *J. Polym. Sci., Part A: Polym. Chem.*, 1991, **29**, 591-597.

38 V. Percec and J. Heck, *Polym. Bull.*, 1991, **25**, 55-62.

39 V. Percec and J. Heck, *Polym. Bull.*, 1991, **25**, 431-438.

40 V. Percec, J. Heck and G. Ungar, *Macromolecules*, 1991, **24**, 4957-4962.

41 J.-F. Zheng, X. Liu, X.-F. Chen, X.-K. Ren, S. Yang and E.-Q. Chen, *ACS Macro Lett.*, 2012, **1**, 641-645.

42 X.-Q. Liu, J. Wang, S. Yang and E.-Q. Chen, *ACS Macro Lett.*, **2014**, **3**, 834-838.

43 H.-T. Nguyen, C. Destrade and J. Malthécte, *Adv. Mater.*, 1997, **9**, 375-388.

44 A. M. Levelut, J. Malthěte, C. Destrade and N. H. Tinh, *Liq. Cryst.*, 1987, **2**, 877-888.

45 J. Malthěte, H. T. Nguyen and C. Destrade, *Liq. Cryst.*, 1993, **13**, 171-187.

46 H. T. Nguyen, C. Destrade and J. Malthète, *Liq. Cryst.*, 1990, **8**, 797-811.

47 C. Alstermark, M. Eriksson, M. Nilsson, C. Destrade and H. T. Nguyen, *Liq. Cryst.*, 1990, **8**, 75-80.

48 M. Gharbia, A. Gharbi, H. T. Nguyen and J. Malthête, *Curr. Opin. Colloid Interface Sci.*, 2002, **7**, 312-325.

49 Y. Yu, M. Nakano and T. Ikeda, *Nature*, 2003, **425**, 145.

50 N. I. Boiko, M. A. Bugakov, E. V. Chernikova, A. A. Piryazev, Ya. I. Odarchenko, D. A. Ivanovb, and V. P. Shibaeva, *Polym. Chem*., 2015, **6**, 6358–6371.

51 V. Percec and B. Hahn, *Macromolecules*, 1989, **22**, 1588-1599.

52 N. Hosono, T. Kajitani, T. Fukushima, K. Ito, S. Sasaki, M. Takata and T. Aida, *Science*, 2010, **330**, 808-811.

53 H. Tu, X. Wan, Y. Liu, X. Chen, D. Zhang, Q.-F. Zhou, Z. Shen, J. J. Ge, S. Jin and S. Z. D. Cheng, *Macromolecules*, 2000, **33**, 6315-6320.

54 J. Brandrup, E. H. Immergut and E. A. Grulke, *Polymer Handbook, 4th ed.*, A Wiley-Interscience Publication, 2003.

55 K. Tashiro, S. Sasaki and M. Kobayashi, *Macromolecules*, 1996, **29**, 7460-7469.

Synthesis and Self-Organization of Azobenzene Containing Hemiphasmidic Side-Chain Liquid-Crystalline Polymers with Different Spacer Lengths

Yan-Shuang Xu,[a] Dong Shi,[a] Jun Gu,[b] Zhen Lei,[a] He-Lou Xie,[c] Ti-Peng Zhao,[a] Shuang Yang,*[,a] and Er-Qiang Chen*[,a]

[a] *Beijing National Laboratory for Molecular Sciences, Department of Polymer Science and Engineering and Key Laboratory of Polymer Chemistry and Physics of Ministry of Education, College of Chemistry and Molecular Engineering, Center for Soft Matter Science and Engineering, Peking University, Beijing 100871, China*

[b] *State Key Laboratory of Rare Earth Materials Chemistry and Applications, College of Chemistry and Molecular Engineering, Peking University, Beijing 100871, China*

[c] *Key Laboratory of Special Functional Polymer Materials of Hunan Province, College of Chemistry, Xiangtan University, Xiangtan 411105, Hunan Province, China*

Email address: eqchen@pku.edu.cn; shuangyang@pku.edu.cn

Hemiphasimidic side-chain liquid-crystal polymers form different columnar phases depending on the spacer length *n* and temperature *T*.

Table of Content